AUG 8 1974

AEDC-TR-74-40 **Unclassified**

cy. 6

DOC NUM SER CN
UNC03667 PDC B 1

ELECTRON DENSITY PROFILE MEASUREMENTS

Joseph A. Sprouse and J. D. Few
ARO, Inc.

ENGINE TEST FACILITY
ARNOLD ENGINEERING DEVELOPMENT CENTER
AIR FORCE SYSTEMS COMMAND
ARNOLD AIR FORCE STATION, TENNESSEE 37389

June 1974

Final Report for Period November 1, 1972 — May 31, 1973

Approved for public release; distribution unlimited.

Prepc . . . Air Force
F40600-74-C-0001

Prepared for

ARNOLD ENGINEERING DEVELOPMENT CENTER (DYFS)
ARNOLD AIR FORCE STATION, TN 37389

Unclassified

NOTICES

When U. S. Government drawings specifications, or other data are used for any purpose other than a definitely related Government procurement operation, the Government thereby incurs no responsibility nor any obligation whatsoever, and the fact that the Government may have formulated, furnished, or in any way supplied the said drawings, specifications, or other data, is not to be regarded by implication or otherwise, or in any manner licensing the holder or any other person or corporation, or conveying any rights or permission to manufacture, use, or sell any patented invention that may in any way be related thereto.

Qualified users may obtain copies of this report from the Defense Documentation Center.

References to named commercial products in this report are not to be considered in any sense as an endorsement of the product by the United States Air Force or the Government.

APPROVAL STATEMENT

This technical report has been reviewed and is approved.

Marshall K Kingery

MARSHALL K. KINGERY
Research and Development
Division
Directorate of Technology

Robert O Dietz

ROBERT O. DIETZ
Director of Technology

UNCLASSIFIED

SECURITY CLASSIFICATION OF THIS PAGE (When Data Entered)

REPORT DOCUMENTATION PAGE		READ INSTRUCTIONS BEFORE COMPLETING FORM
1. REPORT NUMBER AEDC-TR-74-40	2. GOVT ACCESSION NO.	3. RECIPIENT'S CATALOG NUMBER
4. TITLE (and Subtitle) ELECTRON DENSITY PROFILE MEASUREMENTS		5. TYPE OF REPORT & PERIOD COVERED Final Report - Nov 1, 1972, to May 31, 1973
		6. PERFORMING ORG. REPORT NUMBER
7. AUTHOR(s) Joseph A. Sprouse and J. D. Few		8. CONTRACT OR GRANT NUMBER(s)
9. PERFORMING ORGANIZATION NAME AND ADDRESS Arnold Engineering Development Center Arnold Air Force Station, TN 37389		10. PROGRAM ELEMENT, PROJECT, TASK AREA & WORK UNIT NUMBERS Program Element 62302F Project No. 5730 Task 9
11. CONTROLLING OFFICE NAME AND ADDRESS Arnold Engineering Development Center (DYFS), Arnold Air Force Station, TN 37389		12. REPORT DATE June 1974
		13. NUMBER OF PAGES 38
14. MONITORING AGENCY NAME & ADDRESS(if different from Controlling Office)		15. SECURITY CLASS. (of this report) UNCLASSIFIED
		15a. DECLASSIFICATION/DOWNGRADING SCHEDULE N/A

16. DISTRIBUTION STATEMENT (of this Report)

Approved for public release; distribution unlimited.

17. DISTRIBUTION STATEMENT (of the abstract entered in Block 20, if different from Report)

18. SUPPLEMENTARY NOTES

Available in DDC.

19. KEY WORDS (Continue on reverse side if necessary and identify by block number)

microwave attenuation	plume models
plasma devices	electron density
electromagnetic fields	arc jet
rocket exhaust plumes	spectrometer

20. ABSTRACT (Continue on reverse side if necessary and identify by block number)

Electron density profiles of a low density supersonic argon plasma were obtained using 35-GHz microwave attenuation data and spectral intensity measurements of the 4158- and 6032-Å argon emission lines. The integrated profile data from the spectral intensity and microwave attenuation measurements were inverted to local values of the emission coefficient and absorption coefficient, respectively, using an Abel inversion technique. The profile data and results of the inversion are presented.

DD FORM 1 JAN 73 1473 EDITION OF 1 NOV 65 IS OBSOLETE

UNCLASSIFIED

SECURITY CLASSIFICATION OF THIS PAGE (When Data Entered)

PREFACE

The work reported herein was conducted by the Arnold Engineering Development Center (AEDC). Air Force Systems Command (AFSC). under sponsorship of the Air Force Rocket Propulsion Laboratory (AFRPL). Edwards Air Force Base, California, under Program Element 62302F, Project No. 5730, Task 9. The results were obtained by ARO, Inc. (a subsidiary of Sverdrup & Parcel and Associates, Inc.), contractor operator of AEDC. AFSC. Arnold Air Force Station, Tennessee. The work was conducted under ARO Project No. RF234, and the manuscript (ARO Control No. ARO-ETF-TR-74-17) was submitted for publication on February 7. 1974.

The authors wish to acknowledge the suggestions of Dr. C. C. Limbaugh in operating the Abel inversion computer code, which he developed. The assistance of Dr. W. K. McGregor, ETF-Projects Branch, ARO, Inc., and Capt. W. Rothchild, Rocket Propulsion Laboratory, is also appreciated.

CONTENTS

Page

1.0 INTRODUCTION 5
2.0 APPARATUS
2.1 Test Cell 8
2.2 Arc Generator and Plasma 9
2.3 Spectrometric Arrangement for Intensity Measurements 10
2.4 35-GHz Plasma Attenuation System 11
3.0 MICROWAVE ATTENUATION CALIBRATION 12
4.0 ABEL INVERSION TECHNIQUE 13
5.0 ELECTRON TEMPERATURE AND NUMBER DENSITY FROM SPECTRAL MEASUREMENTS 15
6.0 SPECTRAL AND MICROWAVE MEASUREMENTS
6.1 Spectral Considerations 16
6.2 Spectral Measurements 17
6.3 Microwave Attenuation Measurements 21
7.0 DISCUSSION OF RESULTS 26
8.0 SUMMARY OF RESULTS 28
REFERENCES 29

ILLUSTRATIONS

Figure

1. Schematic Diagram of the Microwave and Spectral Arrangement Used to Obtain Radial Profile Data from a Low Density Argon Plasma 7
2. Photograph of the R2E-1 Test Cell and Apparatus 7
3. Schematic Sketch of the R2E-1 Test Cell 8
4. Schematic Diagram of the Arc Jet 9
5. Schematic Diagram of an Argon Plasma Free Jet Expanding into a Low Pressure Test Cell 10
6. Schematic Diagram of a Cylindrically Symmetric System Illustrating the Coordinate Notation Used in the Abel Inversion 13
7. Measured Intensity Profiles for the 4158- and 6032-Å Argon Emission Lines 17
8. Emission Coefficient Profiles for the 4158- and 6032-Å Argon Emission Lines . . 18
9. Plasma Electron Temperature Profile from Line Ratio Calculations 19

Figure Page

10. Plasma Electron Density Profile Using Absolute Intensity Measurements of the 4158- and 6032-Å Argon Emission Lines 20
11. Plasma Microwave Attenuation Data 2 in. Downstream of Normal Shock 21
12. Microwave Attenuation Coefficient versus Radius 23
13. Electron Density Calculations versus Attenuation Coefficient for Various Values of Collision Frequency 25
14. Comparison of Plasma Electron Density Profiles Using Microwave Attenuation and Spectral Data 26

TABLE

1. Electron Temperature, Total Electron Collision Frequency, Electron-Ion Collision Frequency, Plasma Frequency, and Electron Densities at Various Radial Positions Approximately 2 in. Downstream of the Mach Disk 27

APPENDIX

A. PLANE ELECTROMAGNETIC WAVES IN A HOMOGENOUS PLASMA 31

NOMENCLATURE 36

1.0 INTRODUCTION

The interaction of plasmas with electromagnetic fields is a topic of considerable breadth and increasing importance. The Air Force Rocket Propulsion Laboratory (RPL) at Edwards Air Force Base is particularly concerned with the interaction of microwave signals and rocket exhaust plumes. It is known that the free electrons in rocket exhaust plumes interact with radar signals and may result in observable plume radar echoes. Also, the plume can severely interfere with the transmission of microwave signals through the plume by attenuating the signal or by phase distortion. It is impractical. if not impossible, to measure the radar cross section (RCS) of all missile plumes over the range of flight conditions of interest. Therefore, accurate and reliable models are required to predict the plume RCS. The problem of predicting plume RCS is twofold. First, the electrical properties of the plume must be modeled. This requires complex gas dynamic and chemical analysis of interactions of the external air mixing with the exhaust plume. Second, the scattering of the microwave signal from these plumes must be modeled from the predicted plume electrical properties. Both plume electrical properties models (Ref. 1) and plume radar scattering models (Ref. 2) exist.

A key parameter in these models is the local value of electron number density. It is therefore necessary to measure the local value of the electron density of plumes in order to verify these models. There are three basic measuring techniques which can be used to obtain plume electron density: (1) probes (e.g., Langmuir probes), (2) spectral emission meaurements, and (3) microwave attenuation or phase shift measurements. The severe environment of rocket exhaust plumes prohibits the use of probes for reliable electron density measurements. For solid rocket motor plumes the unsteadiness of the plume, coupled with solid particulate continuum radiation and the low intensity of the radiation at the desired wavelength from the appropriate atoms, makes it virtually impossible to use spectral emission data for calculating the plume electron density. This therefore dictates that microwave attenuation and/or phase-detecting techniques be used to measure the electron density in solid rocket exhaust plumes.

Additional problems arise when the electron density is not uniform across the plume because the resultant signal represents the integrated effects of the interaction of the transmitted microwave signal and the plume as it passes through the plume. It then becomes necessary to invert the measured data from integrated results to local values of an absorption coefficient. This inversion requires scanning of the microwave beam across the plume, which in turn generates further constraints on the system (e.g., adequate resolution of the density profile requires that the beam diameter must be much smaller than the plume diameter). The plume diameter encountered in most laboratory experiments is relatively small (4 to 8 in.), and it is therefore necessary to have the microwave frequency

as high as possible so that better focusing techniques can be applied. These constraints make it extremely difficult to make phase-shift measurements because of the signal path around the plasma which is required for phase-shift comparison. At the higher frequencies the wave guide becomes quite sensitive to vibrations, and at the lower frequencies resolution is lost. The method of obtaining electron density profiles of rocket exhaust plumes therefore narrows down to using microwave attenuation data where the selection of the microwave frequency is dictated more by resolution requirements than by the plasma frequency.

The primary purpose of the project reported herein was to examine the prospect of obtaining plasma electron number density profiles from microwave attenuation measurements. To accomplish this goal a low density supersonic argon plasma, produced by an arc jet, was used to provide axisymmetric electron density profiles from which spectral data and microwave attenuation data could be obtained. The electron density and temperature profiles were obtained from inversion of the spectral line data, using previously developed methods (Ref. 3) to evaluate the inversion of the integrated attenuation data and the available theories for relating the inverted attenuation data to electron number density. The emphasis of this investigation was to obtain experimental microwave attenuation data under known operating conditions and to use existing relationships to obtain electron density from the attenuated data. It was not the express purpose of this project to delve into the theoretical aspects of waves propagating through real plasmas, but rather to provide good experimental data for present or future evaluation of wave-propagating models. The results of the investigation, however, did point to the necessity for more refined analysis of the wave propagation.

2.0 APPARATUS

The experimental apparatus consisted of an arc jet which exhausted into a low density test cell, a spectroscopic measurement system, and a microwave transmitter and receiver system. The arrangement of the apparatus is shown in Fig. 1. Simultaneous microwave attenuation and spectral measurements were made to avoid the problems associated with trying to establish repeatable plasma conditions. Further, a square, rather than cylindrical, quartz test section was chosen to prevent lens effects as the plume is scanned by either the microwave beam or spectrometer. The microwave system was mounted on a scanning table which is orthogonal to the spectrometer as shown in Fig. 1. The experimental arrangement is further illustrated by the photograph in Fig. 2, and a sketch of the test cell cross section is shown in Fig. 3.

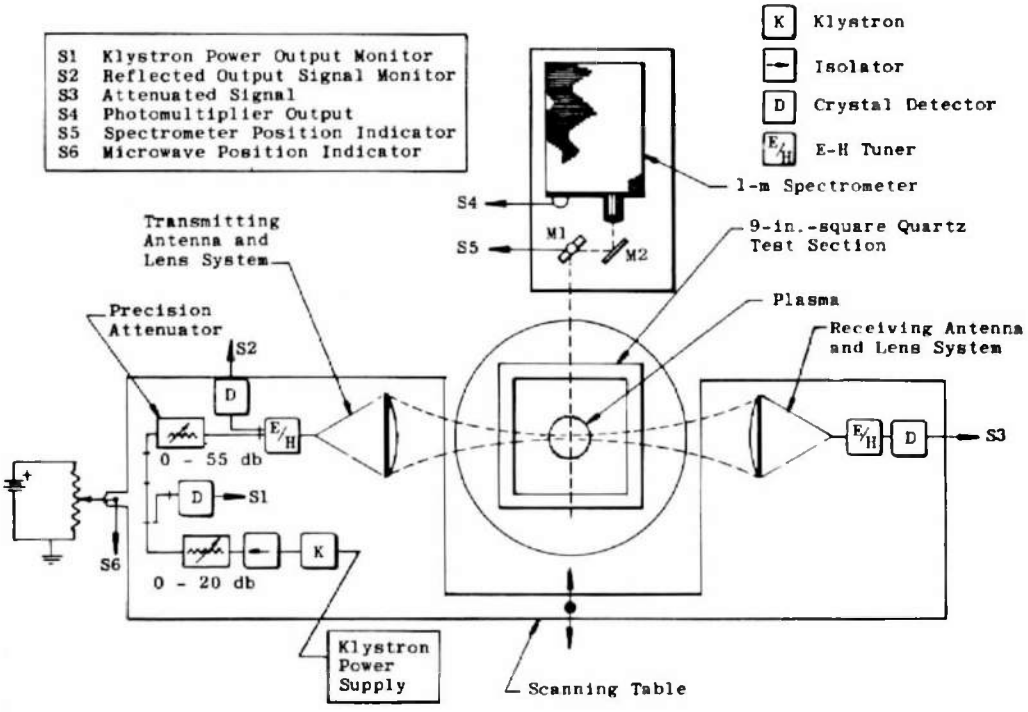

Figure 1. Schematic diagram of the microwave and spectral arrangement used to obtain radial profile data from a low density argon plasma.

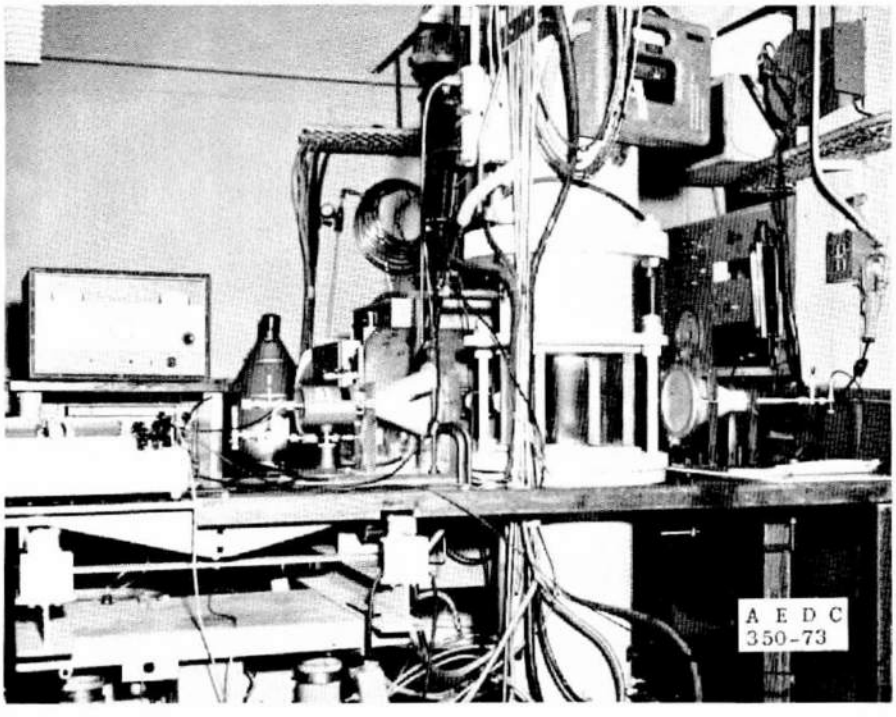

Figure 2. Photograph of the R2E-1 test cell and apparatus.

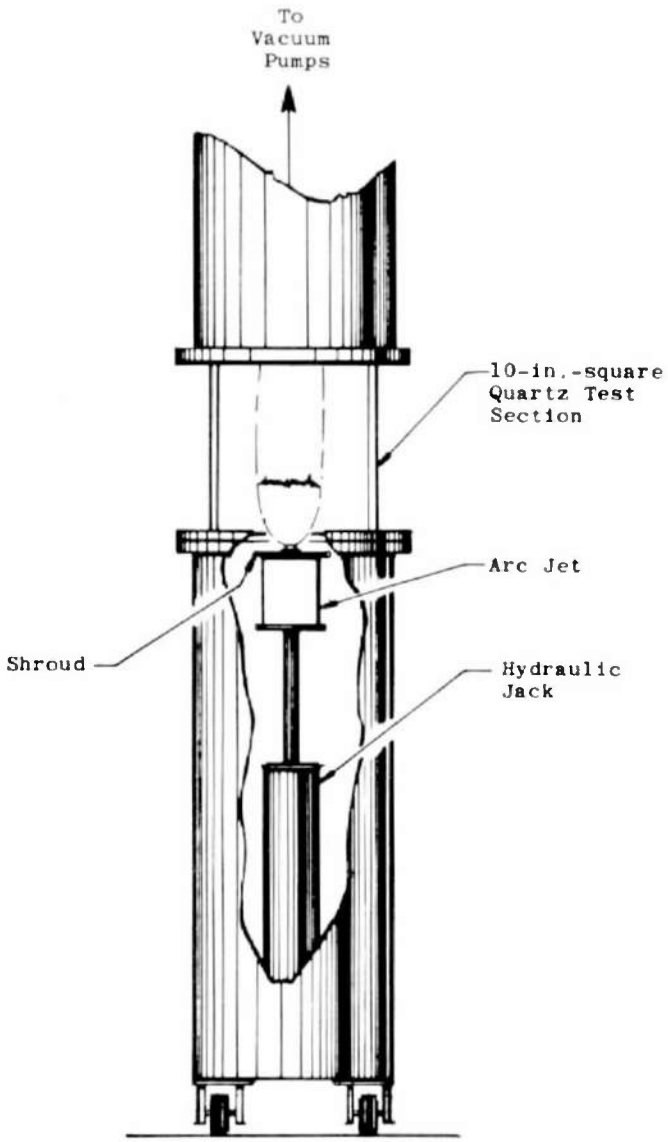

Figure 3. Schematic sketch of the R2E-1 test cell.

2.1 TEST CELL

The viewing section of the test cell was constructed from four pieces of 1-in.-thick optically flat quartz, 9 in. wide and 10 in. high. The 9-in.-square quartz test section was attached to a 12.75 in.-diam section of pipe. The lower section of pipe (approximately 36 in. long) housed the plasma arcjet. The upper section of pipe was connected to vacuum pumps. Test cell pressures as low as 0.01 torr with no flow and 0.6 torr with arc jet and shroud flow could be maintained. A schematic diagram of the test cell and arc jet installation is shown in Fig. 3.

2.2 ARC GENERATOR AND PLASMA

The plasma generator used in these experiments is a Gerdian-type configuration and is fully described in Ref. 4. The arc jet is mounted on a hydraulic jack so that various axial positions of the plasma can be viewed in the test section. The arc jet (Fig. 4) is equipped with a circular shroud made from 1/4-in.-diam steel tubing with several small holes drilled around the perimeter to permit the inclusion of a stream of argon around the argon plasma. The shroud of argon makes the plasma more stable and also reduces the mixing of the plasma with the ambient air in the test section. Typical operating conditions are as follows: arc voltage, 25 v; arc current, 168 amp; chamber pressure, 5 in. Hg; argon flow through arc jet, 0.32 gm/sec, argon flow through shroud, 0.28 gm/sec, test cell pressure, 0.6 torr.

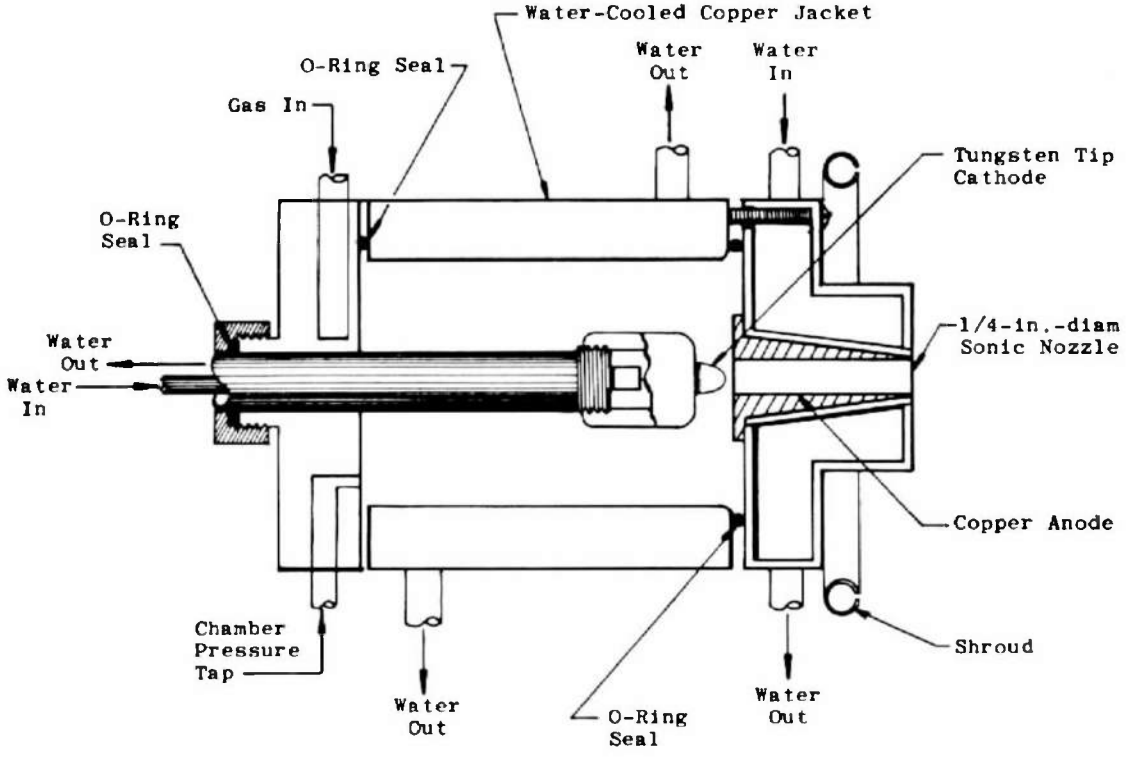

Figure 4. Schematic diagram of the arc jet.

The argon gas enters the arc chamber and expands from a 1/4-in.-diam sonic nozzle into the low pressure test cell after passing through the arc. (The degree of ionization of an argon gas under the operating conditions outlined above ranges from 1 to 5 percent (Ref. 4)). A schematic diagram of a typical supersonic argon plasma is shown in Fig. 5. The supersonic expansion is bounded by a barrel shock up to the Mach disc, and the

flow is subsonic just downstream of the Mach disc. The properties of the flow are considerably different in the region downstream of the normal shock and the region upstream of the normal shock (Ref. 5). Most of the microwave and spectral data were obtained just upstream (Station 1) and just downstream (Station 2) of the Mach disc. (Only the data taken at Station 2 are reported herein because of the difficulty in calculating the collision frequencies in the supersonic region of the plasma jet. Also, the barrel shock in the supersonic regions requires extensive care and preparation to ensure that reliable data from the Abel inversion are obtained.)

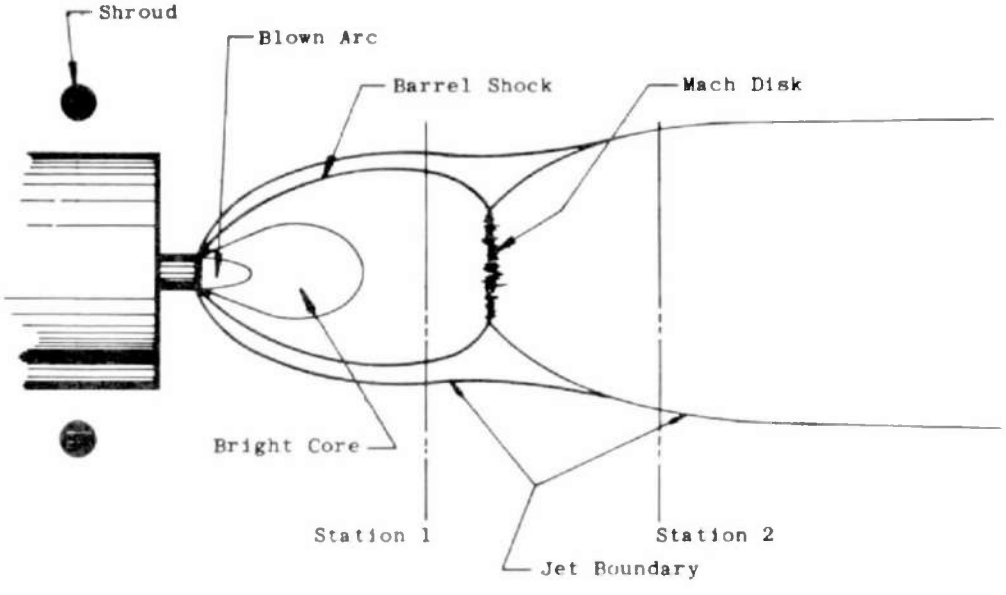

Figure 5. Schematic diagram of an argon plasma free jet expanding into a low pressure test cell.

2.3 SPECTROMETRIC ARRANGEMENT FOR INTENSITY MEASUREMENTS

A 1-m Jarrell-Ash® grating spectrometer with a Czerny-Turner mount was used for the intensity measurements. The spectrometer is equipped with curved slits and 1180 groove/mm grating blazed for maximum reflection at 7500Å. A 40-μ slit was used which gives an equivalent slit width of 0.24Å and a resolution of 0.25Å. An F-8, 35-mm focal length achromatic lens was mounted at the entrance slit of the spectrometer and focused on the plasma centerline.

A pair of plane front surface mirrors, M1 and M2, were located in the optical path as shown in Fig. 1. Mirror M1 could be rotated through a 5-deg angle so that a radial

scan of the plasma could be obtained. The mirror was remotely operated by a synchronous reversible motor. The angular position was monitored with a 1000-Ω linear potentiometer which served as the x-input for the x-y plotter used to record the intensity data. The optical path from mirror M1 to plasma centerline was 24 in., which provided a total radial scan of 6 in. The small angle of deflection coupled with the 24-in. focal length very closely approximates a straight line through the center of the plasma. The measured field of view at the focal point was approximately 1 x 2 mm.

An RCA IP28 photomultiplier was used as the detector. The system was calibrated for absolute intensity by placing a secondary standard tungsten ribbon filament lamp at the focal point of the optics and recording the known intensity over the range of wavelength of interest.

2.4 35-GHz PLASMA ATTENUATION SYSTEM

A schematic diagram of the microwave attenuation system and the hydraulically operated table for scanning the plasma is given in Fig. 1. A forced-air-cooled reflex klystron operating at 400 mw at a frequency of 34.91 GHz provided the microwave power for the experiments. The microwave signal, after leaving the klystron, passes through a ferrite isolator to reduce the strength of any signals which might be reflected back into the klystron. A 0- to 20-db attenuator was added so that the power to the antenna could be adjusted as required. (Generally this attenuator was set at the zero position). The power output was monitored by including a 20-db directional coupler and monitoring the output signal (S1) with a crystral detector. (If the klystron and power supply were turned on 2 hrs prior to testing, it was found that the klystron maintained a steady output with no drift. Therefore, a 2-m warmup period was always observed prior to testing). Following the 20-db coupler is a 0- to 55-db precision attenuator which was used for calibration of the microwave attenuation system. The calibration extended from 0 to 45 db. Another directional coupler was placed after the attenuator and was used to monitor the reflected signal (S2). (The reflected signal mentioned here represents the reflected signals from all points beyond the coupler (e.g., the transition guide, antenna, lens, test cell, etc.), and it serves primarily as an aid in adjusting the E/H tuner for impedance-matching purposes, and not as measure of the reflected signal from the plasma). An E/H tuner was inserted prior to entering the antenna for impedance-matching purposes. The signal was then fed to a dielectric lens-focused antenna, then through the test cell and into the receiving antenna from which the attenuated signal (S3) was monitored.

The focusing antenna consisted of two confocal conical horns (7.032 in. long with an aperture of 6 in., phase corrected with dielectric lens, Rexolite® 1422 (Refs. 6 and 7)). The horn antennas were originally designed for X-band operation; therefore, a transition

section from K- to X-band was required. The antennas used in these experiments were not designed specifically for optimum conditions (i.e., the flare angle of the antenna for either the E or H plane was not chosen for optimum operating conditions (see Refs. 8 and 9). Also, the energy profile emerging from the waveguide is not uniform. These factors result in an uneven illumination of the first lens, and the net effect is that the energy of the beam is concentrated in a narrow beam of approximately 1-cm diameter with a fairly long focal depth. Thus, the system was insensitive to minor variations in focal length. This feature actually simplified the laboratory operation and the analysis because the main body of the microwave energy was concentrated along the microwave antenna centerline in a narrow beam of plane waves as they passed through the plasma.

3.0 MICROWAVE ATTENUATION CALIBRATION

When reflections from plasma boundaries and internal refractions can be neglected, then the plasma can be treated as an insertion loss, and the signal at the receiving antenna can be calibrated by inserting calibrated absorbtion devices into the signal path. (Note: reflections can be neglected if the plasma properties vary slowly with respect to the wavelength of the incoming microwave energy; see Ref. 10.) The microwave system was calibrated in these experiments by inserting a precision attenuator in the system (see Fig. 1) and recording the output signal (S3) as the attenuator was varied from 0 to 45 db. The large range of attenuation represents a power variation of approximately five orders of magnitude, and therefore requires a great deal of care at the higher attenuation values in order to maintain an accurate recording of these calibration points. A high gain amplifier was added at the receiving detector to amplify the signal (S3) at the higher values of attenuation. The addition of the amplifier required that the calibration be performed at several (typically five) known gain settings and that the plasma attenuation data be obtained at the same gain settings.

The operating procedures for calibration were to set the gain of the amplifier and then to set the precision attenuator to a known value. The attenuated signal (S3) and position signal (S6) were recorded on the x-y plotter as the microwave beam was scanned across the test section with no plasma. The attenuated signal was recorded as the y-input on an x-y plotter, and the signal which monitored position of the table (S6) was used as the x-input. The gain was held constant and this procedure repeated for a number of attenuation settings on the precision attenuator. The gain was then increased to a new level and the above procedure repeated until calibration data were obtained over the desired range (typically 0 to 45 db). The precision attenuator was then reset to 0 db in preparation for plasma attenuation measurements.

4.0 ABEL INVERSION TECHNIQUE

The measured intensity of an emission line in an optically thin plasma represents the integrated sum of the emissions of the emitting species along the optical path in the plasma. Similarly, the microwave signal at the receiver end represents the transmitted signal minus the integrated loss of the transmitted signal as it passes through the plasma. If the property being observed (i.e., emission coefficient, absorption coefficient, etc.) is constant along the observation path, the integral is simply the product of the coefficient times the path length. However, when the properties are not uniform along the path of observation, an inversion scheme is required to obtain local values of the properties.

The Abel transformation (Ref. 11) represents a mathematical procedure by which the integrated signal from a cylindrically symmetric source can be transformed into local properties. The main features of this technique are illustrated in Fig. 6. If it can be assumed

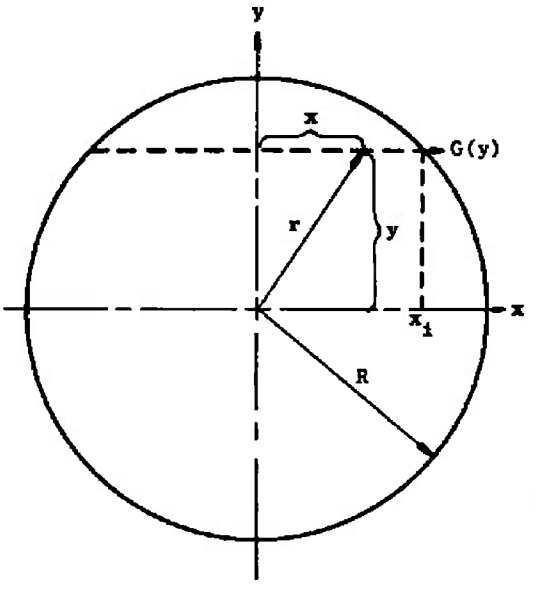

$$G(y) = 2\int_0^{x_i} f(r)\,dx$$

$$x_i = \sqrt{R^2 - y^2}$$

$$x = \sqrt{r^2 - y^2}$$

$$dx = \frac{r\,dr}{\sqrt{r^2 - y^2}}$$

$$\therefore$$

$$G(y) = 2\int_y^R \frac{f(r)\,r\,dr}{\sqrt{r^2 - y^2}}$$

Figure 6. Schematic diagram of a cylindrically symmetric system illustrating the coordinate notation used in the Abel inversion.

that the measured parameter G(y) represents the integrated sum of the local property f(r), then the following analysis may be made:

$$G(y) = \int_{-x_1}^{x_2} f(r)\,dx = 2\int_0^{x_2} f(r)\,dx \qquad (1)$$

where

$$x = \sqrt{r^2 - y^2} \tag{2}$$

and

$$x_1 = \sqrt{R^2 - y^2}$$

The transformation to cylindrical coordinates yields

$$G(y) = 2\int_y^R \frac{f(r)r\,dr}{\sqrt{r^2 - y^2}} \tag{3}$$

Thus under the conditions outlined above, the local plasma parameter, f(r), can be obtained using the Abel transformation as shown below.

$$f(r) = -\frac{1}{\pi}\int_r^R \frac{(dG/dy)dy}{\sqrt{y^2 - r^2}} \tag{4}$$

Many techniques have been developed to perform the inversion calculation of Eq. (4). The choice of technique depends primarily upon the investigator's preference, and to some extent upon the quality of the data. The procedure for evaluating Eq. (4) in this investigation was to represent the measured parameter G(y) (either line intensity or attenuation) by a series of least-square-fit, even-function, sixth-order polynominals and to perform the differentiation and integration analytically using numerical methods. The validity of the curve fit requires data fluctuations to be random. Consequently, it is necessary that several data points at each radial position be input to the computer program in order to obtain an accurate least-square fit to these random data points. However, when the fluctuations in the data are small (i.e., when the data can be characterized by a single curve), then the curve fit must be exact. Otherwise, large fluctuations in the inverted data can be expected. Since the data used in this report were of the latter category (i.e.. exhibiting very small fluctuations), it was necessary to demand a close curve fit (±0.5 percent) to the data points. It was possible to obtain the curve fit within ±0.5-percent tolerances only from the centerline out to approximately 1 cm and within ±5-percent tolerance on out to 10 or 11 cm.

As can be seen from Eq. (4) the coefficient f(r) is functionally related to the spatial derivative of the measured parameter G(y), and it is therefore possible to produce major fluctuations in f(r) with only minor fluctuations in G(y), which is a main weakness of

the inversion technique. In fact, it requires care and skill in order to properly apply any inversion scheme to real cases because of the sensitivity of the inverted results to the quality of the measured data.

5.0 ELECTRON TEMPERATURE AND NUMBER DENSITY FROM SPECTRAL MEASUREMENTS

The electron temperature and density of an electrically neutral plasma for which the upper energy states of the excited argon are in a Boltzmann distribution are related according to Saha's equation (Ref. 12).

$$n_e^2 = \left(\frac{2\pi m_e k T_e(r)}{h^2}\right)^{3/2} N_n \frac{2Z_{A+}^{elec}}{Z_A^{elec}} \exp\left[-(E_I - E_n)/k T_e(r)\right] \tag{5}$$

For a given atom there are two unknowns in this equation; N_n (the number of atoms which are in the energy state E_n) and T_e (the electron temperature). Thus two parameters must be measured to obtain the electron number density[1]. The measurement of the intensity of two emission lines is sufficient to obtain these parameters. That is, the power radiated per unit volume per unit solid angle at a given wavelength is

$$\epsilon_{nm} = \frac{hc}{4\pi\lambda} N_n A_{nm} \tag{6}$$

where ϵ_{nm} is often called the emission coefficient, λ is the wavelength, and A_{nm} is the transition probability associated with the transition to E_n (Ref. 11). The intensity of the radiation at the spectrometer is

$$I_{nm}(y) = 2\int_0^{x_1} \epsilon_{nm}\, dx \tag{7}$$

Use of the Abel transform (see Eqs. (4) and (6)) yields

$$N_n(r) = \frac{4\lambda}{hc A_{nm}} \int_R^r \frac{(dI_{nm}/dy)dy}{\sqrt{y^2 - r^2}} \tag{8}$$

---

[1] If the energy states were in equilibrium down to the ground state, it would be possible to calculate N_n from pressure and electron temperature data. For low density Argon plasmas this is seldom true.

The ratio of the emission coefficients of two argon lines labeled 1 and 2 can be used to obtain the electron temperature (Ref. 11).

$$T_e(r) = \frac{(E_2 - E_1)/k}{\ln\left(\frac{\epsilon_1}{\epsilon_2}\right)\left(\frac{g_2 A_2 \lambda_1}{g_1 A_1 \lambda_2}\right)} \tag{9}$$

where E is the energy of the upper state, k is Boltzmann's constant, g is the statistical weight, A is the transition probability, and λ is the wavelength. The emission coefficients of the radiation for the two different emission lines subscripted 1 and 2 are

$$\epsilon_1(r) = \frac{1}{\pi} \int_R^r \frac{(dI_1/dy)dy}{\sqrt{y^2 - r^2}} \tag{10}$$

and

$$\epsilon_2(r) = \frac{1}{\pi} \int_R^r \frac{(dI_2/dy)dy}{\sqrt{y^2 - r^2}} \tag{11}$$

6.0 SPECTRAL AND MICROWAVE MEASUREMENTS

6.1 SPECTRAL CONSIDERATIONS

Originally it was planned to use three or four argon emission lines in order to obtain an average value of temperature and electron density at each radial position in the plasma. In practice, however, this proved to be difficult because of the low intensity of some lines of interest which originated from states near the continuum, and also because it was necessary to keep the measuring time to a minimum in order to reduce the possible variations in the data which might result from plasma and instrumentation drift. The spectral response of the photomultiplier also constrains the selection of useful emission lines.

The 4158-, 6032-, and 6965-Å lines were chosen. It was subsequently discovered, however, that the assumption of optically thin plasma and/or Boltzmann distribution was not applicable for the 6965-Å line. The characteristic flatness of the intensity profile in the data obtained with this line indicated that self-absorption might be occurring. The low values of electron temperature consistently obtained when the data from the 6965-Å line were used for temperature calculations generated doubt as to whether the upper energy state associated with this line was in a Boltzmann equilibrium distribution with the other

upper energy states. Thus the 6032- and 4158-Å lines were used in this report to obtain electron temperature and electron density profiles.

6.2 SPECTRAL MEASUREMENTS

The spectrometer was carefully adjusted so that the peak intensity of each line of interest was established, and then the plasma was scanned by rotating the rotating mirror M1 (see Fig. 1) and recording the photomultiplier output (S4) on an x-y plotter. The plasma was scanned several times for each line being observed to ensure repeatability. This procedure was repeated for each emission line of interest. The measured intensity data obtained were used in the Abel inversion program, for which the emission coefficient for each line, the electron temperature, and electron number density were calculated.

The measured intensity profiles of the 4158- and 6032-Å lines taken at Station 2 (approximately 2 in. downstream of the Mach disk) are shown in Fig. 7. The error boundaries (indicated by the dashed lines in Fig. 7) were obtained from the error bounds quoted for the calibration curve which was used to convert the recorded photomultiplier voltage to radiant intensity units. Instrumentation errors were neglected because the same instruments were used under identical circumstances for intensity calibration and for plasma spectral measurements. The inverted emission coefficients, with the indicated error bounds for these two coefficients, are shown in Fig. 8. The error bounds shown in Fig. 8 for

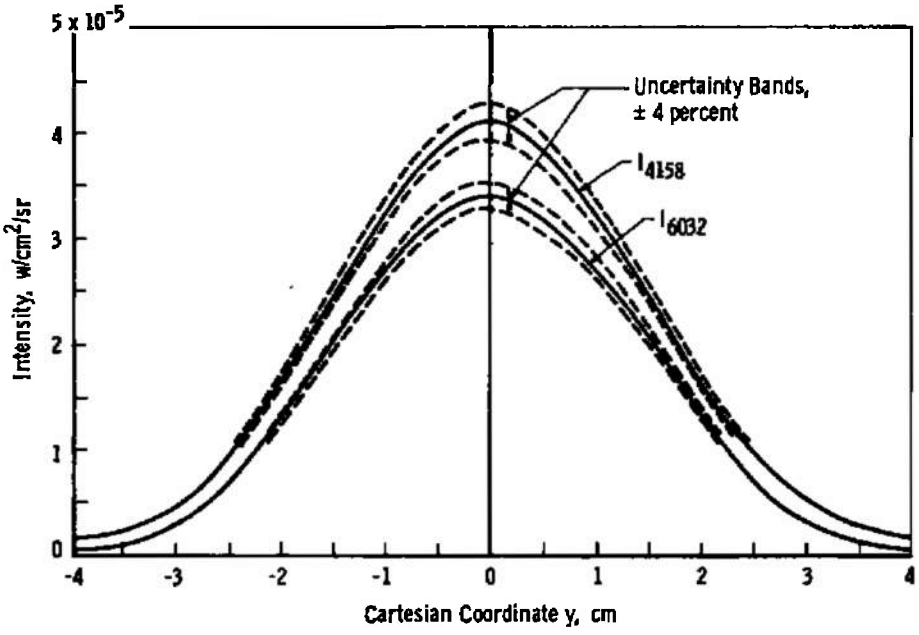

Figure 7. Measured intensity profiles for the 4158- and 6032-Å argon emission lines.

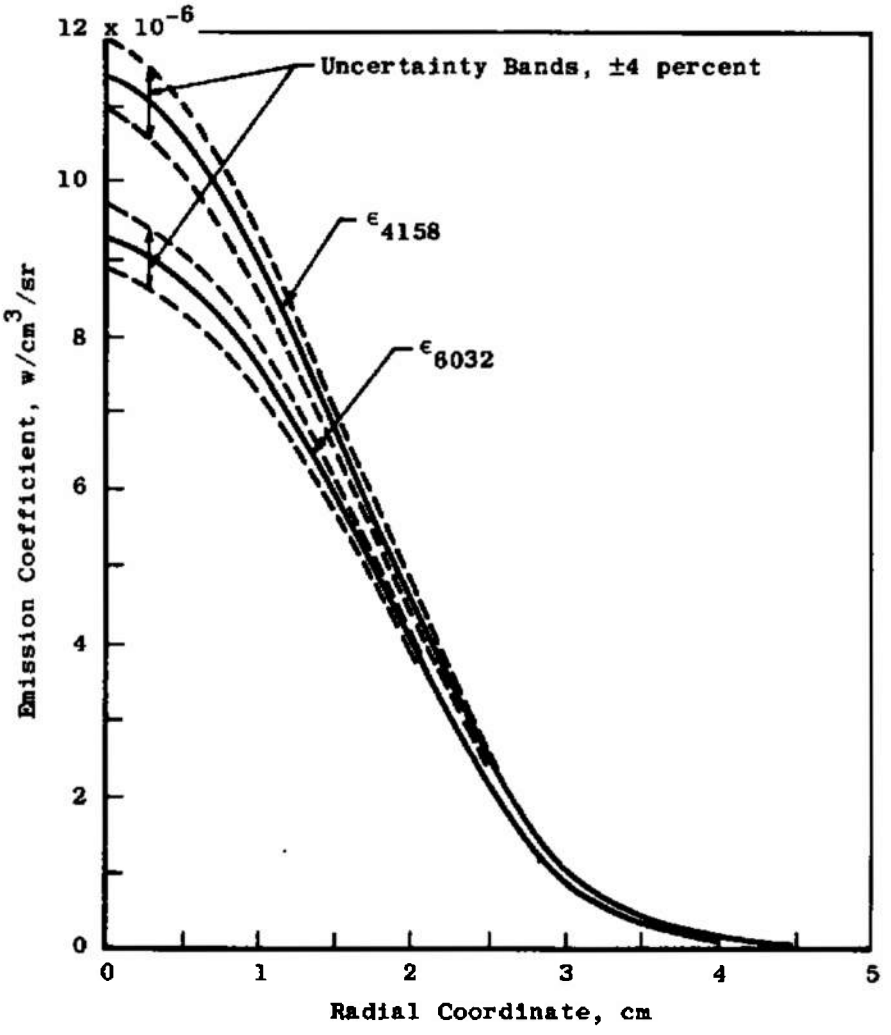

Figure 8. Emission coefficient profiles for the 4158- and 6032-Å argon emission lines.

the emission coefficients are the same as those for the intensity curve; that is, it is assumed that the inversion process does not generate any additional error. and therefore, that the error bounds should be the same for both the intensity and the emission coefficients. The electron temperature and electron number density using 4158- and 6032-Å emission data lines are shown in Figs. 9 and 10, respectively. The principal factors which contribute to the uncertainty in the electron temperature are the transition probability uncertainties (±5 percent for the 4158-Å transition and ±5 percent for the 6032-Å transition (Ref. 13)) and the uncertainty associated with the emission coefficients (±4 percent). (The

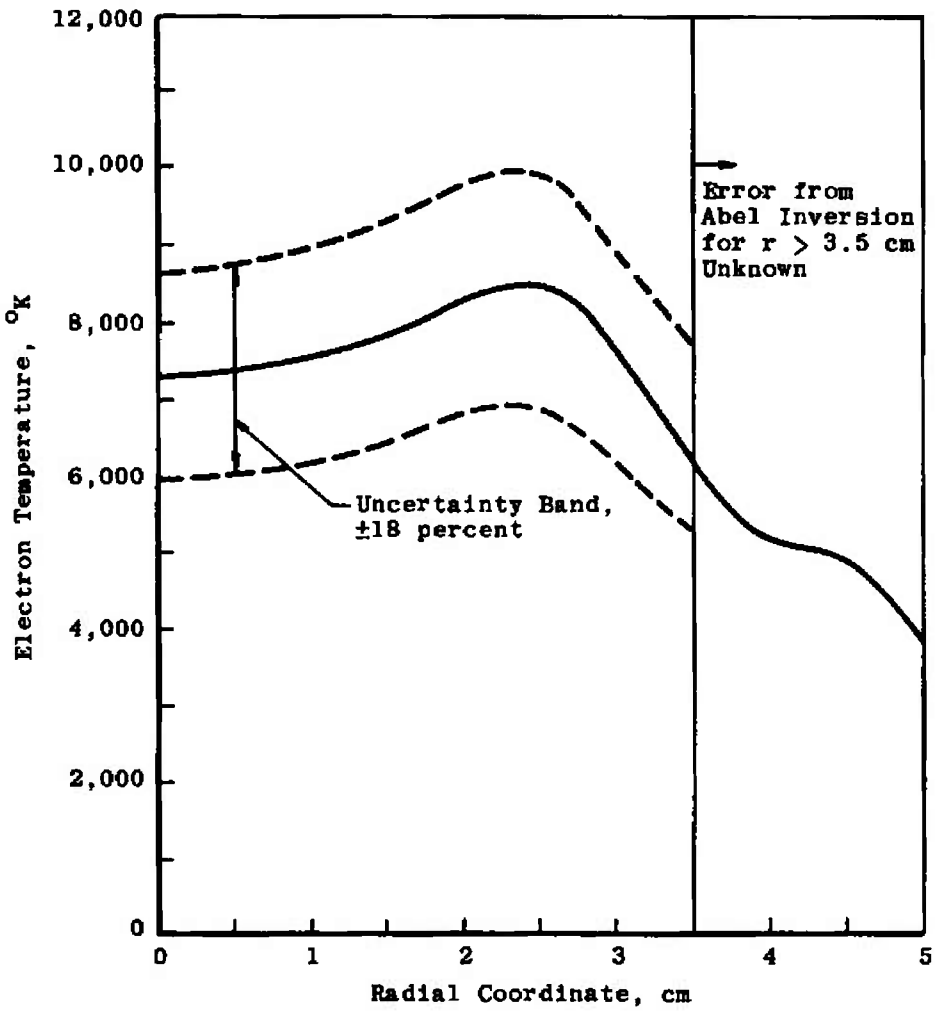

Figure 9. Plasma electron temperature profile from line ratio calculations.

±4-percent uncertainty in the emission coefficients is based upon the uncertainty associated with the secondary tungsten filament used for absolute intensity calibrations (±3 percent) and reproduction uncertainty (±1 percent)). The errors combine to give an uncertainty in the electron temperature obtained for line ratio calculations of approximately ±18 percent. The uncertainty in the electron number density obtained from absolute line intensity measurements can be traced to the uncertainty in the transition probability (±5 percent), emission coefficients (±4 percent), and electron temperature (±18 percent). The net effect of these errors is to produce an uncertainty of ±36 percent in the electron density obtained from spectroscopic data.

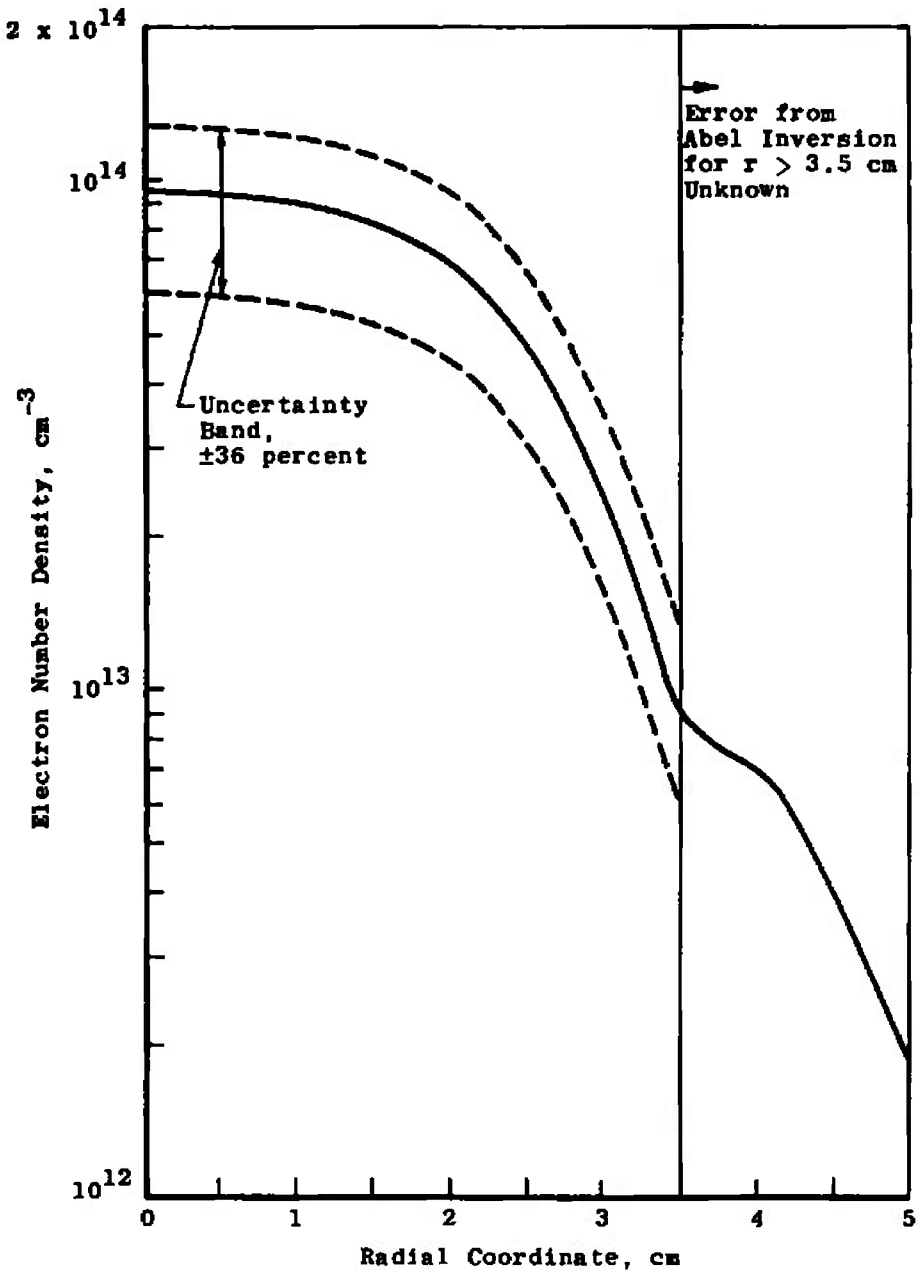

Figure 10. Plasma electron density profile using absolute intensity measurements of the 4158- and 6032-Å argon emission lines.

6.3 MICROWAVE ATTENUATION MEASUREMENTS

6.3.1 Measuring Procedures

The test cell was evacuated and the microwave system was calibrated as outlined in Section 3. Next the plasma flow was initiated, and the plume was positioned in the test cell so that the desired axial position along the plasma could be viewed. The microwave attenuation data were then recorded on an x-y plotter as the microwave beam was scanned radially across the plasma. This procedure was repeated for each value of amplifier gain used during the system calibration. The attenuation profile was obtained by superimposing the calibration curves onto the measured data. A representative attenuation profile obtained by this procedure is shown in Fig. 11. The overlapping data points observed result from the overlap obtained at adjoining gain positions used in calibration and data acquisition.

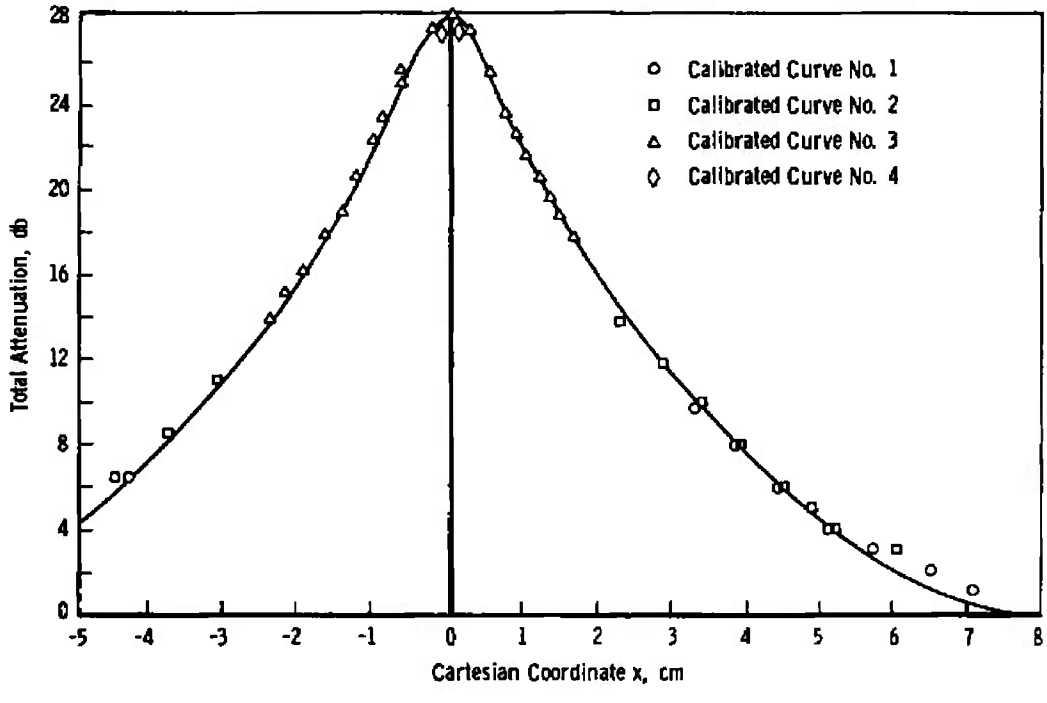

Figure 11. Plasma microwave attenuation data 2 in. downstream of normal shock.

The uncertainty in the attenuation data can be traced to the uncertainty in the precision attenuator (Fig. 1) which was used for calibration purposes and to the random error

generated in the data acquisition process. The total error associated with the attenuation data is estimated to be approximately ±5 percent.

6.3.2 Attenuation Coefficient

The attenuation profile shown in Fig. 11 represents the integrated attenuation of the microwave signal as it passes through the plasma. Many authors (e.g. see Refs. 14, 15, and 16) have used a rather simple relationship between the measured integrated attenuation and the attenuation coefficient (see Appendix A), and in these cases the process of obtaining the inverted data becomes a straightforward procedure. That is, ordinary Abel inversion techniques are applicable. Thus, when it is assumed that the microwave power P_{out} exiting the absorbing medium is given by

$$P_{out} = P_{IN} \exp\left[-\int \alpha dy\right] \tag{12}$$

(where P_{IN} is the input microwave power, and the line integral of the attenuation coefficient is taken over the ray path—see Ref. 16), then the attenuation in units of decibels becomes

$$A(x) = 10 \log_{10}\left(\frac{P_{out}}{P_{IN}}\right) = -4.343 \int_{\ell} \alpha dy \tag{13}$$

For a cylindrically symmetric plasma, Eq. (13) becomes

$$A(x) = -(2)(4.343) \int_{o}^{Y} \alpha(r) dy \tag{14}$$

It is noted that Eq. (14) is of the standard Abel form, and therefore the attenuation coefficient can be obtained quite easily (see Section 4). That is,

$$\alpha(r) = \frac{1}{4.343\pi} \int_{r}^{R} \frac{(dA/dx)dx}{\sqrt{x^2 - r^2}} \tag{15}$$

The numerical procedure for evaluating this expression is outlined in Section 5. The radial profile of the attenuation coefficient for the measured integrated attenuation shown in Fig. 11 for the conditions outlined above is presented in Fig. 12.

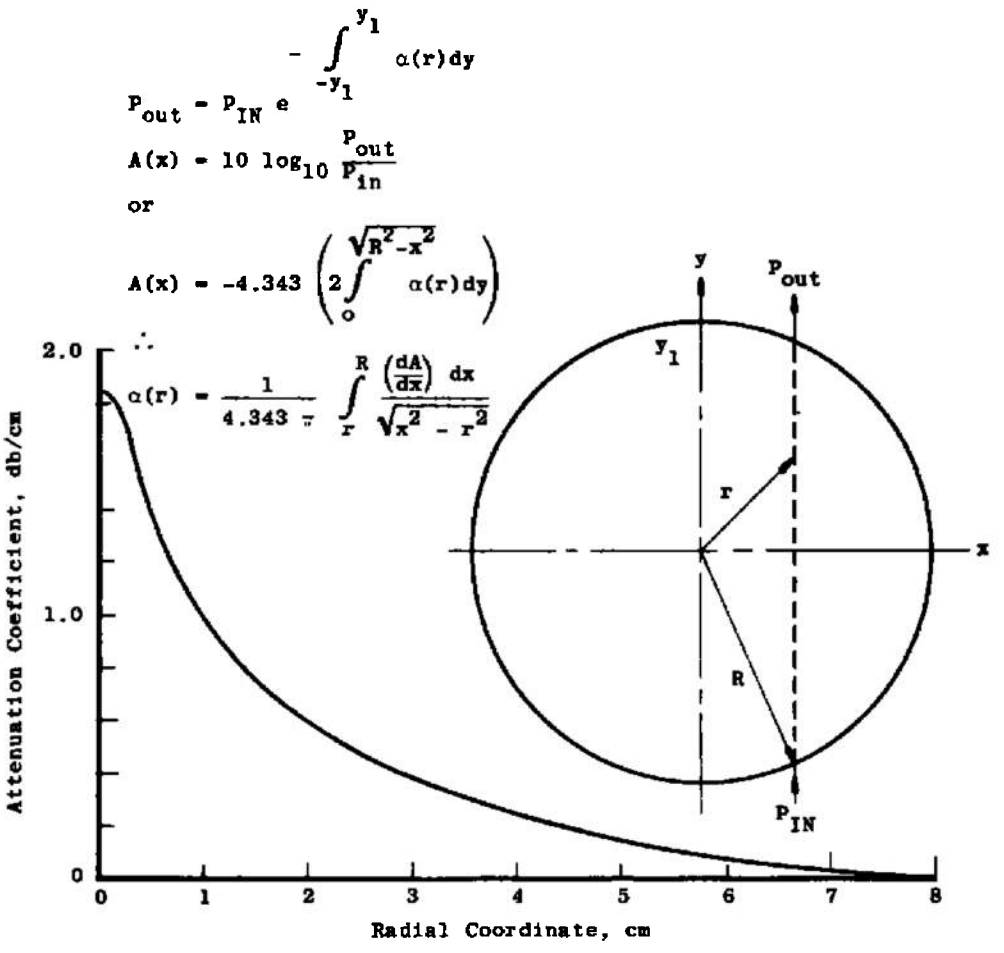

Figure 12. Microwave attenuation coefficient versus radius.

6.3.3 Collision Frequency

In order to calculate the electron density from the attenuation coefficient it is also necessary to either measure or calculate the electron collision frequency. For a pure argon plasma there is sufficient data extant (Ref. 17) so that reliable equations can be used to calculate the collision frequency (Ref. 7). Only two types of encounters need be considered: (1) encounters between electrons and neutral argon atoms, and (2) encounters between electrons and argon ions. (Electron-electron encounters do not change the transport of charge, and therefore may be ignored). That is, the collision frequency ν can be written as the sum of the electron-neutral collision frequency ν_{en} and the electron-ion collision frequency ν_{ei} (Ref. 10). Thus,

$$\nu = \nu_{en} - \nu_{ei} \tag{16}$$

where

$$\nu_{en} = 2.6 \times 10^4 Q_{en} n_g T_e^{1/2} \tag{17}$$

and

$$\nu_{ei} = 3.63 \times 10^{-6} (n_e T_e^{-3/2}) \ln \Lambda$$

$$\Lambda = 1.23 \times 10^4 T_e^{3/2} n_e^{-1/2} \tag{18}$$

Values for the collision cross section, Q_{en}, as a function of electron temperature, T_e, were obtained from Ref. 17. (The electron temperature was determined from the spectral data). The gas density, n_g, at Station 2 was obtained by assuming that the static pressure in the stream is equal to the test cell pressure and assuming that the gas temperature is approximately equal to the total temperature (Ref. 5).

6.3.4 Electron Density

The relationship between the electron density, n_e, and the attenuation coefficient, α, is as follows (see Appendix A):

$$\alpha = \frac{\omega}{\sqrt{2}\, c} \left[\sqrt{(1 - P_I)^2 + P_R^2} - (1 - P_I) \right]^{1/2} \tag{19}$$

where c is the speed of light, ω is the microwave frequency, m_e is the electron mass, and

$$P_I = \frac{n_e e^2}{m_e \epsilon_o (\omega^2 + \nu^2)} \tag{20}$$

and

$$P_R = \frac{\nu}{\omega} P_I \tag{21}$$

The electron number density, n_e, may be calculated directly from Eq. (19) using the relationships established between n_e, P_R, and P_I in Eqs. (20) and (21). That is,

$$n_e = \left(\frac{2c^2 m_e \epsilon_o}{e^2}\right)\left(1 + \frac{\omega^2}{\nu^2}\right)\alpha^2\left[\sqrt{1 - \frac{\nu^2}{\alpha^2 c^2}\left(1 + \frac{\alpha^2 c^2}{\omega^2}\right)} - 1\right] \tag{22}$$

In the limit $\nu^2 << \omega_P^2 << \omega^2$ (where $\omega_P = (n_e e^2/m_e \epsilon_o)^{1/2}$ = plasma frequency), an approximate expression for α can be obtained from Eq. (19) (Ref. 14). That is,

$$\alpha \cong 4.62 \times 10^{-5} \frac{n_e \nu}{\omega^2 + \nu^2} \tag{23}$$

Solving for n_e.

$$n_e \cong 2.165 \times 10^4 \alpha\left(\frac{\omega^2 + \nu^2}{\nu}\right) \tag{24}$$

Since the collision frequency is also a function of the electron density, it is necessary to use an iterative scheme to obtain n_e versus α (see Section 6.3.3). Equations (22) and (24) are plotted in Fig. 13 for various values of ν. In this figure it can be seen that the approximate expression for n_e (see Eq. (24)) asymptotically approaches the exact expression (see Eq. (22)) when $\omega >> \omega_P$ for values of $\nu < \omega$. However, for $\omega < \omega_P$ the approximate expression differs greatly from the exact expression.

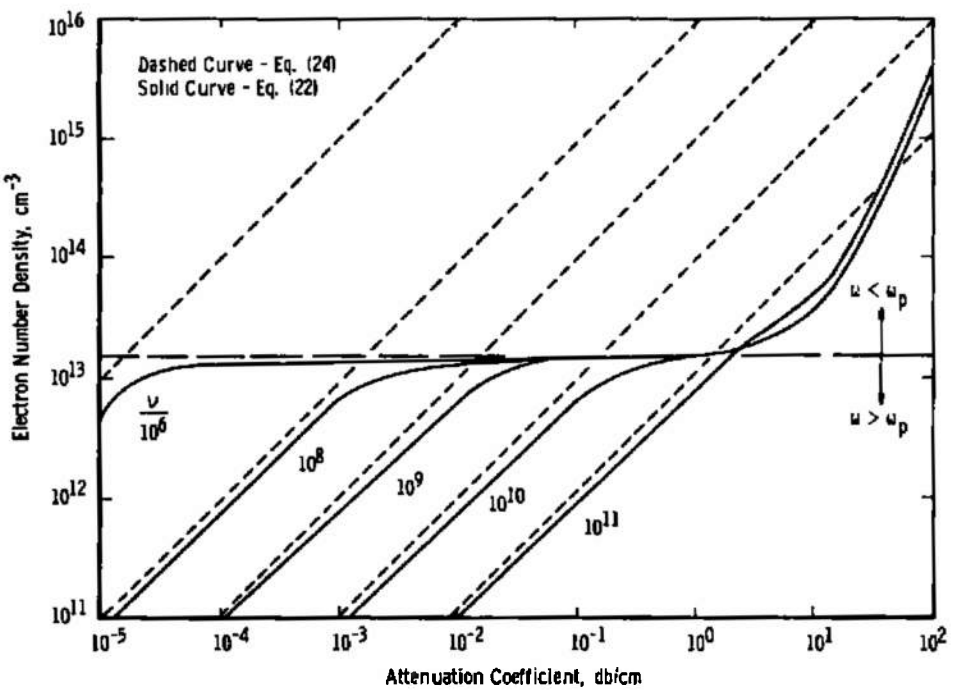

Figure 13. Electron density calculations versus attenuation coefficient for various values of collision frequency.

7.0 DISCUSSION OF RESULTS

The radial profiles of electron density obtained from the spectroscopic data (Fig. 10) and the profiles obtained from the microwave data in conjunction with Eqs. (22) and (24) are compared in Fig. 14. The error bounds for the electron densities obtained

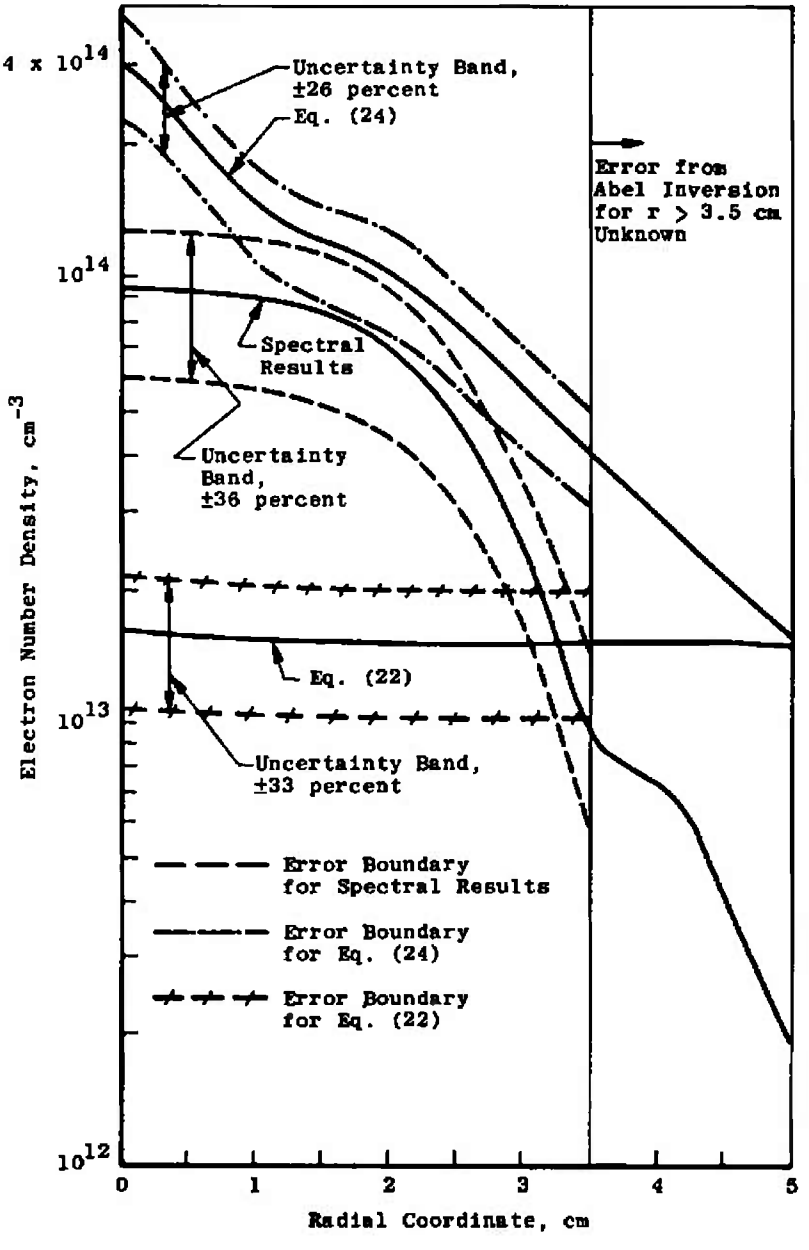

Figure 14. Comparison of plasma electron density profiles using microwave attenuation and spectral data.

from microwave attenuation measurement result from uncertainties in the value of the absorbtion coefficient and the electron temperature. The error bounds for the electron density are ±33 percent using Eq. (22) and ±26 percent using Eq. (24). The plasma electron density profiles obtained from the microwave measurements (either Eq. (22) or Eq. (24)) do not agree with the electron density obtained from spectral measurements. The difference between the profiles obtained from microwave measurements (see Eqs. (22) and (24)) can be explained by noting that for the plasma conditions at Station 2 the limits specified in the simplified expression for electron density (Eq. (24)) are not applicable.

The values of the electron temperature, T_e, total collision frequency, ν, electron-ion collision frequency, ν_{ei}, angular plasma frequency, ω_P, electron density, n_e (Eq. 22), and the values of electron density obtained from spectral measurements at various radial positions, r, are tabulated for the argon plasma at Station 2 (Fig. 5) in Table 1. Examination of this table shows that the limits required for Eqs. (23) and (24) to be applicable are not satisfied.

Table 1. Electron Temperature, Total Electron Collision Frequency, Electron-Ion Collision Frequency, Plasma Frequency, and Electron Densities at Various Radial Positions Approximately 2 in. Downstream of the Mach Disk

r, Radial Position, cm	T_e, Electron Temperature, °K	ν, Total Collision Frequency, $sec^{-1} \times 10^8$	ν_{ei}, Electron-Ion Frequency, $sec^{-1} \times 10^8$	ω_P, Plasma Frequency, $rad/sec \times 10^{11}$	n_e, Eq (22), $cm^{-3} \times 10^{13}$	n_e, Spectral, $cm^{-3} \times 10^{13}$
0.0	7312	7.14	7.07	2.27	1.62	9.35
0.5	7375	6.95	6.87	2.24	1.58	9.18
1.0	7600	6.52	6.44	2.21	1.54	8.70
1.5	7880	6.19	6.11	2.21	1.53	8.05
2.0	8225	5.84	5.75	2.20	1.52	6.92
2.5	8375	5.70	5.61	2.20	1.52	5.20
3.0	7480	6.57	6.49	2.20	1.52	2.55
3.5	6150	7.89	7.83	2.20	1.52	0.89
4.0	5150	9.79	9.74	2.20	1.51	0.74
4.5	4850	12.30	12.23	2.19	1.50	0.41
5.0	3820	15.20	15.14	2.17	1.47	0.19
5.5	3200	18.50	18.49	2.12	1.41	0.10

The difference between the spectral results and the microwave results (particularly those obtained using the exact expression given by Eq. (22)) are more difficult to explain. It is possible that the results obtained from spectral data are not correct. However, a more likely explanation of the difference is that the microwave equations (Eqs. (22) and (24)) which are used to relate the attenuation coefficient to the integrated total attenuation are not applicable to inhomogeneous media. First of all, Eq. (13) is based upon a plane

wave passing through a uniform conductive media (see Appendix A) and not upon the case in which $\vec{\nabla}\sigma \neq o$ (i.e., the propagation coefficient in the wave equation is not constant).

Since the microwave beam cross section (approximately 1-cm diameter) is much larger than the spectral cross section (1 x 2 mm), it is reasonable to expect that some differences in the density profiles obtained from microwave and spectral data would exist. That is, the larger aperture associated with the microwave system is more effective at averaging out sharp changes in the density profile. Although the averaging effect could account for some of the discrepancies between the density profile obtained from spectral measurements and the density profile obtained from microwave measurements (Eq. (22)) (particularly toward the outer boundaries of the plasma), averaging cannot account for the large difference (approximately a factor of five) at the plasma centerline.

Other sources of microwave error can arise from reflections which occur at sharp boundaries and from signal scattering in the plasma. A cylindrical plasma in conjunction with a confocal microwave system makes it extremely difficult to measure the reflected signal because of the geometry of the relecting angles. However, unless the plasma boundaries are very sharp (i.e., unless electron density changes rapidly in distances of less than a wavelength), boundary reflections should be minimal (Ref. 10).

The express purpose of this project was to make simultaneous measurements of the plasma electron density profile using spectral data and microwave data with the intent of checking the microwave calculations against the calculations obtained from spectral data. The primary purpose was not to resolve any existing differences but rather to provide reliable experimental data from which further studies might be obtained.

8.0 SUMMARY OF RESULTS

The special arrangement of the microwave and spectral instrumentation along with the test cell configuration offered an ideal opportunity to obtain reliable spectral and microwave attenuation data. For the most part, the integrated intensity profiles and the microwave attenuation profiles were symmetrical about the axis of the plasma; therefore, the inversion of the data could be obtained by straightforward procedures.

The calculation of the electron density profiles from these data (spectral versus microwave) did not agree. The large error bounds for the calculations of electron number density indicate the problem of attempting to make a clear-cut comparison between electron density calculations based on microwave attenuation and spectral line emission data. The large error bounds for the electron density calculations are based upon the

uncertainty in the basic physical constants associated with transitions between excited states for argon. The uncertainty in the collision frequency is the principle factor which contributes to the uncertainty in the microwave electron density calculations. The collision frequency uncertainty can be traced to the uncertainty in the electron temperature, and therefore, the calculations of electron density from microwave attenuation calculations, in this instance, are also subject to the uncertainty attributed to basic physical constants of the argon emission lines. The situation becomes even worse when the plasma is composed of gases more complex than an argon plasma. Other methods of obtaining the collision frequency for more accurate electron density measurements by microwave attenuation techniques are needed.

REFERENCES

1. Smoot, L. D. and Underwood, D. L. "Prediction of Microwave Attenuation Characteristics of Rocket Exhausts." J. Spacecraft and Rockets, Vol. 3, No. 3, March 1966, pp. 302-309.

2. Poehler, H. A. "Project See-Thru Flame Interference Measurements, Titan IIIC Launch Test 8275/2250, Final Report." Pan American World Airways, ASD, Patrick AFB, Fla., ETR-TR-68-3, March 1968.

3. McGregor, W. K. and Brewer, L. E. "Equivalence of Electron and Excitation Temperatures in an Argon Plasma." The Physics of Fluids, Vol. 9, No. 4, April 1966, pp. 826-827.

4. Bryson, R. J. and Frölich, J. P. "Study of the Energy Addition Process in a D-C Arc-Jet." AEDC-TR-65-268 (AD631591), April 1966.

5. Bryson, R. J. "A Method for Determining the Bulk Properties of Arc-Heated Argon." AEDC-TR-69-125 (AD689178), June 1969.

6. Darlington, C. R., Bahor, L. R., and Sprouse, J. A. "Attenuation of Microwaves Transmitted Through the Exhaust Plumes of Solid-Propellant Rocket Motors Operating in a Simulated Flight Environment of Mach Numbers 0.38, 2.0, and 3.0." AEDC-TR-71-259 (AD891998L), February 1972.

7. Mayfield, D. A. and Hendrix, R. E. "Microwave Focusing Techniques and Their Early Applications in the VKF." AEDC-TM-66-4, January 1966.

8. Microwave Antenna Theory and Design. Edited by Samuel Silver. McGraw-Hill Book Company, Inc., New York. 1949.

9. Kraus, J. D. Antennas. McGraw-Hill Book Company, Inc., New York, 1950.

10. Shkarofsky, I. P., Johnston. T. W., and Bachynski, M. P. The Particle Kinetics of the Plasmas. Addison-Wesley Publishing Company, Ontario. 1966.

11. Griem, H. R. Plasma Spectroscopy McGraw-Hill Book Company, Inc., New York, 1964.

12. Cambel, A. B. Plasma Physics and Magnetofluid-Mechanics. McGraw-Hill Book Company, Inc., New York, 1963

13. Adcock, B. D. and Plumbtree, W. E. G. "On Excitation Temperature Measurements in a Plasma-Jet, and Transition Probabilities for Argon Lines." Journal of Quantitative Spectroscopy and Radiative Transfer, Vol. 4, No. 1, 1964, pp. 29-39.

14. Heald, M. A. and Wharton, C. B. Plasma Diagnostics with Microwaves. John Wiley and Sons, Inc., New York, 1965.

15. Smoot, L. D. and Seliga, T. J., Jr. "Rocket Exhaust Plume Radar Attenuation and Amplitude/Phase Noise." J. Spacecraft and Rockets. Vol. 4, No. 6. June 1967, pp. 774-780.

16. Williams, H. and Wilson, A. S. "The Measurement of Radial Electron Density Profiles in Rocket Exhaust Jets." R.I.W.G. Report No. 02/70, August 1970.

17. Massey, H. S. W. and Burhop, E. H. S. Electronic and Ionic Import Phenomena. Oxford University Press. London. 1952.

APPENDIX A
PLANE ELECTROMAGNETIC WAVES IN A HOMOGENEOUS PLASMA

Maxwell's equations in an isotropic plasma and for time-harmonic variations of the form exp (-jωt) may be written

$$\overrightarrow{\nabla \times \vec{E}} = j\omega\vec{B} \tag{A-1}$$

$$\overrightarrow{\nabla \times \vec{B}} = (\omega^2\mu_0\epsilon_0 - j\omega\mu_0\sigma)\frac{\vec{E}}{\mu\omega} - \frac{k^2\vec{E}}{j\omega} \tag{A-2}$$

$$\vec{\nabla} \cdot \vec{E} = 0 \tag{A-3}$$

$$\vec{\nabla} \cdot \vec{B} = 0 \tag{A-4}$$

where $j = \sqrt{-1}$ and $k = (\omega^2\mu_0\epsilon_0 + j\omega\mu_0\sigma)^{1/2}$ propagation coefficient. The constitutive equation, $\vec{D} = \epsilon_0\vec{E}$, $\vec{B} = \mu_0\vec{H}$ and Ohm's law $\vec{J} = \sigma\vec{E}$ were used to obtain this particular form of Maxwell's equations. The free-space values of permittivity $\epsilon_0 = 1/36\pi \times 10^{-9}$ F/m and the free-space value of permeability $\mu_0 = 4\pi \times 10^{-7}$ hy/m were used for the plasma. The equation for the propagation of the electric field through the plasma is obtained by taking the curl of Eq. (A-1) and eliminating $\vec{B}$ using Eq. (A-2). That is,

$$\overrightarrow{\nabla \times (\nabla \times \vec{E})} = \vec{\nabla}(\vec{\nabla} \cdot \vec{E}) - \nabla^2\vec{E} = k^2\vec{E} \tag{A-5}$$

Since $\vec{\nabla} \cdot \vec{E} = 0$ in a plasma, the wave equation for the electric field propagating through a plasma is

$$\nabla^2\vec{E} + k^2\vec{E} = 0 \tag{A-6}$$

Similarly, the wave equation for the magnetic field is obtained by taking the curl of Eq. (A-2). Thus

$$\overrightarrow{\nabla \times (\nabla \times \vec{B})} = \vec{\nabla}(\vec{\nabla} \cdot \vec{B}) - \nabla^2\vec{B} = \frac{\overrightarrow{\nabla \times k^2\vec{E}}}{\mu\omega} \tag{A-7}$$

where

$$\overrightarrow{\nabla \times k\vec{E}} = k^2\overrightarrow{(\nabla \times \vec{E})} - \vec{E} \times \overrightarrow{\nabla k^2} \tag{A-8}$$

The wave equation for the magnetic field is obtained from Eqs. (A-2), (A-4), (A-7), and (A-8). That is,

$$\nabla^2\vec{B} + k^2\vec{B} + \frac{\overrightarrow{(\nabla k^2 \times E)}}{j\omega} = 0 \tag{A-9}$$

where

$$\overrightarrow{\nabla k^2} = j\omega\mu_0\overrightarrow{\nabla\sigma}$$

Thus, Eq. (A-9) can be written as

$$\nabla^2\vec{B} - k^2\vec{B} + \mu_0\overrightarrow{(\nabla\sigma \times E)} = 0 \tag{A-10}$$

It can be seen from Eq. (A-10) that when the gradient of the conductivity is not zero, the equations for the electric and magnetic fields are coupled and nonlinear. A nonzero conductivity gradient, of course, compounds the problem of calculating the attenuation of the electromagnetic field as it travels through an inhomogeneous plasma because it becomes necessary to know not only the value of k, but also how k varies from point to point in the plasma. However, before pursuing the problem of calculating the fields and attenuation for the inhomogeneous case, it is instructive to first look at the homogeneous case.

It is convenient to divide the complex propagation coefficient, k, into real and imaginary components. Before this is done, however, it is necessary to note that the conductivity is also complex. For a Lorentz plasma (i.e., one where the collision frequency is independent of velocity[1]), the electrical conductivity is of the form (Ref. 14)

$$\sigma = \frac{n_e e^2}{m_e}\left(\frac{1}{\nu - j\omega}\right) = \sigma_R + j\sigma_I \tag{A-11}$$

Thus the propagation coefficient, k, is

$$k = [(\omega^2\mu_0\epsilon_0 - \omega\mu_0\sigma_I) + j\omega\mu_0\sigma_R]^{1/2} = \beta + j\alpha \tag{A-12}$$

where α is the attenuation coefficient and β is the phase coefficient. Solving for α and β in Eq. (A-12) yields

$$\alpha = \frac{\omega}{\sqrt{2}c}\left[\sqrt{(1 - P_I)^2 + P_R^2} - (1 - P_I)\right]^{1/2} \tag{A-13}$$

[1]The velocity here is the average directed velocity for the electron ensemble and not the rms random velocity.

and

$$\beta = \frac{\omega}{\sqrt{2}c}\left[\sqrt{(1-P_I)^2 + P_R^2} + (1-P_I)\right]^{1/2} \tag{A-14}$$

where

$$P_I = \sigma_I/\omega\epsilon_0 \qquad \text{and} \qquad P_R = \sigma_R/\omega\epsilon_0$$

The terminology used to denote α and β becomes evident when plane wave solutions to the wave equations (Eqs. (A-6) and (A-10)) are obtained for a homogeneous plasma. The electric and magnetic fields for a plane electromagnetic wave traveling in the z direction in a homogeneous plasma (e.g., $\vec{\nabla}\sigma = 0$) which are solutions to the wave equations are

$$\vec{E}(z,t) = \vec{i}_x E_0 \exp\left[-\alpha z - j(\omega t - \beta z)\right] \tag{A-15}$$

and

$$\vec{B}(z,t) = \vec{i}_y \frac{E_0\sqrt{\alpha^2+\beta^2}}{\omega} \exp\left[-\alpha z - j(\omega t - \beta z - \theta)\right] \tag{A-16}$$

where E_0 is value of the electric field at $z = 0$ and $\theta = \tan^{-1}(\alpha/\beta)$ (Note: only the real part of these expressions is used in computing the values of E or B.) Equations (A-13) and (A-16) represent solutions to the wave equations in which the fields are attenuated by the factor $\exp(-\alpha z)$ and phase shifted by the factor $\exp(-j\beta z)$ as the electromagnetic wave propagates through the plasma in the z direction.

The attenuation of a microwave signal as it passes through a lossy medium in units of decibels (db) is defined as

$$A(db) = -10 \log_{10}\left(\frac{P_{out}}{P_{IN}}\right) \tag{A-17}$$

where P_{out} is the electromagnetic power emerging from the lossy medium and P_{IN} is the power entering the medium. These powers can be calculated quite simply for a cylindrical microwave beam of radius b propagating through a homogeneous plasma of length ℓ as depicted in Fig. (A-1). The power flowing through surface S_1 is

$$P_{IN} = \iint_{S_1} \left\langle \frac{\vec{E}_I \cdot \vec{B}_I}{\mu_0} \right\rangle \cdot \vec{dS}_1 \tag{A-18}$$

and the power flowing through surface S_2 is

$$P_{out} = \iint_{S_2} \left\langle \frac{\overrightarrow{E_2 \times B_2}}{\mu_o} \right\rangle \cdot \vec{dS}_2 \tag{A-19}$$

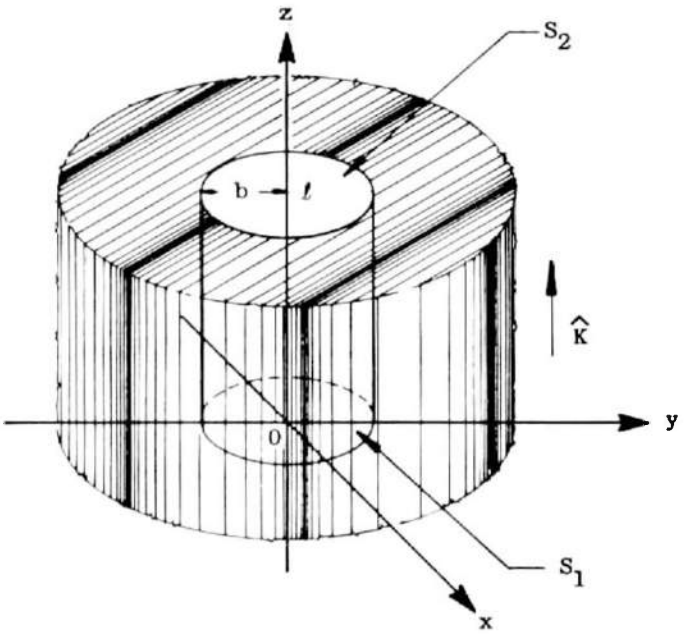

Figure A-1. Cylindrical microwave beam with radius b traveling through a homogeneous plasma.

where the subscripts 1 and 2 refer to the value of the electromagnetic fields at surfaces S_1 and S_2 respectively. The brackets $< >$ signify time-averaged values. For the cylindrical geometry depicted in Fig. (A-1) the elements of surface area dS_1 and dS_2 are defined as

$$\vec{dS}_1 = \vec{dS}_2 = \vec{i}_z r d\theta dr \tag{A-20}$$

The electric and magnetic fields at S_1 (i.e., z = 0) are

$$\vec{E}_1(0,t) = \vec{i}_x E_o \cos(\omega t) \tag{A-21}$$

and

$$\vec{B}_1(0,t) = \vec{i}_y \frac{E_o}{\omega} [\beta \cos(\omega t) - \alpha \sin(\omega t)]$$

Therefore,

$$P_{IN} = \frac{\beta E_o^2}{2\omega\mu_o} \int_o^{2\pi} \int_o^b r d\theta dr = \pi b^2 \left(\frac{\beta E_o^2}{2\omega\mu_o}\right) \tag{A-22}$$

The electric and magnetic fields at S_2 (i.e., $z = \ell$) are

$$\vec{E}_2(\ell,t) = \vec{i}_x E_o e^{-\alpha\ell} \cos(\omega t - \beta\ell) \tag{A-23}$$

and

$$B_2(\ell,t) = \vec{i}_y \frac{E_o e^{-\alpha\ell}}{\omega} [\beta \cos(\omega t - \beta\ell) + \alpha \sin(\omega t - \beta\ell)]$$

Therefore,

$$P_{out} = \frac{\beta E_o^2 e^{-2\alpha\ell}}{2\omega\mu_o} \int_o^{2\pi} \int_o^b r d\theta dr = \pi b^2 \left(\frac{\beta E_o^2 e^{-2\alpha\ell}}{2\omega\mu_o}\right) \tag{A-24}$$

The attenuation in units of db is

$$A(db) = -10 \log_{10}\left(\frac{P_{out}}{P_{IN}}\right) = 20\alpha\ell \log_{10} e = 8.686\, \alpha\ell \tag{A-25}$$

It should be emphasized that the derivation of Eq. (A-25) is based upon the propagation of a plane electromagnetic wave through a homogeneous plasma for which Ohm's law ($\vec{J} = \sigma\vec{E}$) is applicable. (Also, boundary effects have been ignored in this derivation). The important condition here, however, is homogeneousness of the plasma (i.e., $\vec{\nabla}\sigma = 0$). This aspect is often overlooked (see for example, Ref. 16). Thus the inversion of the total attenuation A(db) into an absorption coefficient using this expression is subordinate to these conditions. The error in neglecting these conditions has yet to be evaluated.

NOMENCLATURE

A_{nm}	Transition probability for transitions from the nth level energy state to the mth level energy state
$A(x)$	Microwave attenuation, $10 \log_{10} (P_{out}/P_{IN})$
c	Speed of light in a vacuum, 2.9979×10^8 m/sec
E_I	Ionization energy level
E_n	Energy of the nth level
e	Charge on electron 1.6021×10^{-19} coulombs
$G(y)$	$2 \int_0^{x1} f(r)\ dx$
g_n	Degeneracy of the nth energy state
h	Plank's constant, 6.6256×10^{-27} erg-sec
I_{nm}	Intensity of the radiation from nth energy level
j	$\sqrt{-1}$
m_e	Mass of electron, 9.1091×10^{-31} kg
n_e	Electron number density
n_g	Heavy particle number density
P_{IN}	Microwave input power to plasma
P_{out}	Microwave power at exit of plasma
Q_{en}	Electron-neutral collision cross section
R	Radius of the plasma
r	Radial coordinate
T_e	Electron temperature
x,y	Cartesian coordinates

$Z_{A^+}^{elec}$	Electron partition function for the ionized atom
Z_A^{elec}	Electron partition function for the neutral atom
$\alpha(r)$	Microwave attenuation coefficient
ϵ_{nm}	Emission coefficient for spectral emission from upper energy state n to lower energy state m
ϵ_o	Free-space permittivity, $10^{-9}/36\pi$ f/m
Λ	$1.23 \times 10^7\ T_e^{3/2}\ n_e^{-1/2}$
λ	Wavelength
μ_o	Free-space permeability, $4\pi \times 10^{-7}$ hy/m
ν	Total collision frequency, $\nu_{ei} + \nu_{en}$
ν_{ei}	Electron-ion collision frequency
ν_{en}	Electron-neutral collision frequency
σ	Electrical conductivity
ω	Angular frequency of microwave signal
ω_p	Angular plasma frequency, $(n_e e^2/m_e \epsilon_o)^{1/2}$